AIAA JOURNAL
Vol. 47, No. 9, September 2009

Mode Conversion in Acoustically Modulated Confined Jets

N. Noiray,* D. Durox,† T. Schuller,‡ and S. Candel§
Ecole Centrale Paris, Laboratoire d'Energetique Moleculaire et Macroscopique, Combustion, Centre National de la Recherche Scientifique, 92295 Châtenay-Malabry, France

DOI: 10.2514/1.37734

This paper is concerned with the response of confined low-Reynolds-number jets to external modulations of large amplitudes. The jet formed inside a duct by an orifice plate is submitted to flow perturbations impinging on the constriction from the upstream side. Vortices are generated in the downstream region, giving rise to conversion from acoustic oscillation to convective modes. Experiments and simulations are carried out to characterize this important mode conversion process. It is shown that the convective perturbation phase is a linear function of the distance from the orifice plate and of the operating frequency. Data can be collapsed into a single curve with some scatter providing a scaling rule for the phase. Numerical simulations are carried out and a method is developed to decompose the local velocity perturbations into acoustic and convective components. This is used to determine the amplitudes of upstream and downstream acoustic velocities and of the convective perturbations on the downstream side of the orifice. It is shown that the acoustic velocity approximated by a bulk oscillation in the orifice vicinity is reduced at the constriction and that this is simultaneously compensated by the generation of convective perturbations. The conversion efficiency of this process is characterized. Results obtained can be used to design flow control devices; they provide insight into the generation of vortices in orifice plate systems submitted to large pressure oscillations and could be useful to the analysis of vortex instabilities in segmented solid rocket engines.

I. Introduction

MECHANISMS governing mode conversion in shear flows are of fundamental and technical interest. It is, for example, important to determine the receptivity of a shear layer to external acoustic perturbations [1] or to define the response of a nozzle or blade row to impinging entropy or vorticity waves [2–5]. Mode conversion that takes place when a freejet is submitted to acoustic perturbations has been envisaged to control sound radiation [6–8]. Bias flow perforated grids are considered in sound control applications for their acoustic damping properties [9,10]. The present investigation is concerned with the conversion process that takes place when acoustic perturbations propagate in an internal flow and impinge on an orifice plate.

This study is motivated by an application to the passive control of combustion instabilities. This is described in Noiray et al. [11,12] and is briefly described herein. The principle of the device developed to this purpose and designated as a dynamical phase converter (DPC) in the aforementioned references is to convert acoustic perturbations into a convective mode. It is then shown that this can be used to adjust the convective delay to dynamically control the motion of the flame formed by an injector. In multipoint injection configurations, the concept requires relatively simple geometrical alterations of injection channels. It is shown that this can be used to obtain a neutral response of combustion to incident acoustic waves. The central idea of the DPC is to modify within a short distance ($\approx$1 cm) the phase angle of incident acoustic perturbations, which modulate a low-Mach-number flow inside a channel. Because the acoustic wavelengths of interest ($\lambda_{ac} = c/f \approx 1$ cm) are very long, it is not possible to obtain a sizeable phase shift within a short distance for this mode of propagation. One may, however, circumvent this problem by first converting the incoming perturbation into a hydrodynamic mode. This is achieved by means of a bias flow orifice, a constriction that is traversed by a mean flow as illustrated in Fig. 1. When acoustic modulations impinge on this orifice from upstream, they trigger the shedding of coherent vortices in the confined jet shear layer. The convection velocity $\mathcal{U}_{cv}$, of these hydrodynamic perturbations is typically close to the mean flow velocity $\bar{u}_d$ in the orifice. Considering that the Mach number is small $M \ll 1$, the "vortex mode wavelength" $\lambda_{cv} = \mathcal{U}_{cv}/f$ is much smaller than the acoustic wavelength λ_{ac}. It is then easier to obtain significant changes of the phase angle between the incident acoustic perturbation $u'_{0,ac}$ and the resulting hydrodynamic fluctuation $u'_{1,cv}$ within a short distance. This can be demonstrated by comparing the acoustic and hydrodynamic phase shifts corresponding to an axial distance z. Assuming that the acoustic mode propagates at the speed of sound c and that the hydrodynamic mode travels at the convection velocity $\mathcal{U}_{cv}$, one finds the following:

$$\varphi_{ac} = \arg\left(\frac{u'_{1,ac}}{u'_{0,ac}}\right) \approx \frac{2\pi f z}{c} \quad \text{and} \quad \varphi_{cv} = \arg\left(\frac{u'_{1,cv}}{u'_{0,ac}}\right) = \frac{2\pi f z}{\mathcal{U}_{cv}} \quad (1)$$

The ratio of these phase shifts $\varphi_{cv}/\varphi_{ac} = 1/M_{cv}$ is equal to the inverse of the convective Mach number $M_{cv} = \mathcal{U}_{cv}/c$, which is small in most injection systems $M_{cv} \ll 1$; correspondingly, the convective phase shift is much larger than the acoustic phase shift. This indicates that the convective mode can be used to adjust the delay and develop a DPC. This, however, requires that the jet established in the duct be receptive to the incident modulation, a property that clearly depends on the Strouhal number [6]. Although the process has been extensively investigated in the case of freejets (see Birbaud et al. [13] for recent experiments), mode conversion is less well documented in the confined case [14]. It is known that the vortex generation process can be quite effective, yielding annular vortices and associated hydrodynamic velocity fluctuations $u'_{1,cv}$ dominating the acoustic component $u'_{1,ac}$ over a wide range of Strouhal numbers. The resultant velocity field on the downstream side of the orifice ($u'_1 = u'_{1,ac} + u'_{1,cv} \simeq u'_{1,cv}$) features a significant phase difference $2\pi f z/\mathcal{U}_{cv}$ with respect to the incident acoustic modulation u'_0. The conversion process operates in the orifice plate vicinity. Further downstream, annular vortices are dissipated by viscosity and the remaining fluctuating velocity is, again, purely acoustic. One aim of this paper is to characterize this unsteady flow in the orifice near field and, in particular, determine the convection velocity and conversion

Received 26 March 2008; revision received 20 October 2008; accepted for publication 9 December 2008.

*Research Fellow, Centre National de la Recherche Scientifique.
†Senior Research Scientist, Centre National de la Recherche Scientifique.
‡Assistant Professor, Ecole Centrale Paris.
§Professor, Ecole Centrale Paris; also Institut Universitaire de France, 103, Boulevard Saint-Michel, 75005 Paris, France. Fellow AIAA.

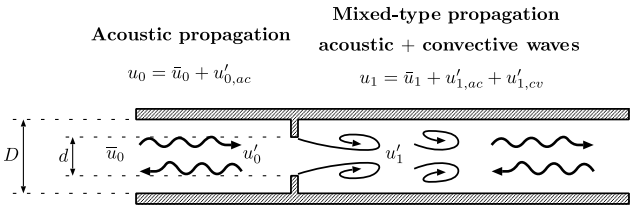

Fig. 1 Representation of an in-duct orifice plate supporting a mean flow ($\bar{u}$) and subjected to an incident acoustic perturbation. Upstream of the orifice, the velocity fluctuations are purely acoustic ($u'_0 = u'_{0,ac}$), whereas the downstream region features acoustic and convective modes ($u'_1 = u'_{1,ac} + u'_{1,cv}$). Vortex structures are convected at a velocity $\mathcal{U}_{cv}$. The orifice discharge flow velocity is $\bar{u}_d = \bar{u}_0/\sigma^2$, where $\sigma = d/D$ is the orifice-diameter-to-duct-contraction ratio.

efficiency of the system for low-Reynolds-number flows under large perturbation amplitudes typical of those encountered inside injectors during unstable combustion.

These quantities are useful to the design of the DPC system, but the results of the present study are also of interest to some other applications:

1) Pulsating jets yielding vortex trains are considered in physiological studies of human speech production, which involves "acoustic-vortex" interactions in the glottis [15]. The analysis of constricted low-Reynolds-number flows under modulation is also of importance for blood circulation in the human body [16].

2) In-duct orifice plates are found in various types of aerospace and mechanical systems. In certain applications, these structural discontinuities are designed to damp acoustic waves, as proposed, for example, by Durrieu et al. [17], who used a prototype of anechoic termination relying on five diaphragms placed in series within a duct. More generally, a theoretical analysis of the acoustic response of a slit shaped diaphragm was proposed by Hofmans et al. [18] in the case of low Strouhal numbers and jet Mach numbers of the order of unity. For low Mach numbers and Strouhal numbers of the order of unity, which correspond to the present situation, numerical simulations have been used to predict the aeroacoustic response of in-duct orifices [19,20]. The role of vortex shedding at the constriction was emphasized in these studies, but the conversion process from acoustic to convective modes was not characterized in detail.

3) Vortex shedding from inhibitors in segmented solid propellant rockets gives rise to low-frequency oscillations that induce undesirable thrust oscillations. Inhibitors protruding in the flow constitute a source of vortices. These vortices impinge on the nozzle generating pressure oscillations. After reflection at the rocket front head, this acoustic wave travels back to the inhibitor. An unstable feedback loop between the vortex shedding and acoustic oscillations can be established, combining hydrodynamic and acoustic modes. A typical experimental result obtained in the case of the Ariane 5 strap-on P230 engine in a static test firing [21,22] indicates that oscillatory pressure amplitudes of 0.5% of the mean pressure yield thrust oscillations of 5% of the mean thrust and an important level of low-frequency accelerations. This mechanism has been extensively investigated. An early interpretation of the phenomenon was proposed by Flandro [23]. Investigations of this process were reviewed by Vuillot [24]. It is shown [25] that adaptive control methods could be used to suppress these self-sustained oscillations. The vortex convection velocity $\mathcal{U}_{cv}$ plays a crucial role in the determination of the possible frequencies of oscillation and the definition of instability onset criteria [26].

As pointed out earlier, acoustic-hydrodynamic conversion at a bias flow constriction is considered for its possible use in acoustic damping devices [27]. A recent theoretical analysis of this problem has led to the derivation of the Rayleigh conductivity of an orifice plate in a duct with flow [28]. This work generalizes Howe's model [29] for an infinite rigid plate featuring an aperture yielding a freejet to the case of a confined jet configurations in which an orifice plate is placed in a channel. Acoustic energy is transferred to a train of vortices generated at the orifice lips, and a net absorption of sound is observed in the conversion process [30]. The same kind of sound absorption mechanism operates in the case of confined jets generated by abrupt area changes [31]. The phase evolution of flow perturbations on the downstream side of the orifice is, however, not considered in these studies. This is an important aspect of the problem as it is related to the convection of vortices shed at the sharp diaphragm edges. It is shown in these previous references that the acoustic conductivity strongly depends on the vortex convection velocity $\mathcal{U}_{cv}$. This velocity $\mathcal{U}_{cv}$ is taken to be half of the mean aperture velocity $\bar{u}_d$ in the freejet aperture case [29], while it is assumed that this quantity is nearly equal to the velocity in the orifice aperture $\mathcal{U}_{cv} = \bar{u}_d$ for confined constrictions [28,31]. In these last configurations, the presence of the wall may be represented by the method of images, and the vortex propagation velocity can be determined by adding image vortices with respect to the wall [32]. The contraction effect of the jet also significantly affects the vortex convection velocity and essentially depends on the shape of the constriction [14,33].

This review of the literature indicates that some useful information is missing. One point of interest is the relation between the vortex convection velocity $\mathcal{U}_{cv}$ and the discharge velocity $\bar{u}_d$. This directly affects the prediction of the acoustic damping properties of bias flow perforated screens. It can be shown that theoretical results are markedly influenced by the value of the convection velocity. From studies on acoustically modulated freejets at low Mach numbers [13], it is known that phase velocities $\mathcal{U}_{cv}$ may take different values in the range $[\bar{u}_d/2,\ \bar{u}_d]$ and that this depends on the jet Strouhal number. This point is less well documented for confined jets. The aim of the present study will be to examine the mechanism that converts incident acoustic perturbations into hydrodynamic fluctuations and measure its efficiency and the resulting convection velocity for low Reynolds number flows. This investigation is first carried out experimentally in a scale-up version of the very small channels considered in the flow control application [11,12] (Sec. II). Experimental phase data described in Sec. III are collapsed into a linear relation that is then used to determine the vortex convection velocity. Simulations are carried out in Sec. IV. A special processing method is developed to identify acoustic and convective components on the downstream side of the orifice plate. This is used to determine the conversion efficiency and obtain estimates of the convective velocity fluctuation on the jet axis. This procedure also yields the convective wave number and axial phase shift. These results are compared with experimental data in the last part of this paper.

II. Experimental Configuration

The experimental setup sketched in Fig. 2 comprises two glass tubes mounted in series on a converging nozzle and connected by a stainless steel orifice plate. The upstream tube is long enough to consider that the flow is fully developed. A driver unit (loudspeaker) is placed at the bottom of the upstream manifold to modulate the flow using harmonic excitations. A laser Doppler velocimetry (LDV) system based on a continuous He–Ne Laser (35 mW, 632 nm) yields velocity measurements on the upstream and downstream sides of the orifice. The Doppler signals are obtained by seeding the flow with micronic oil droplets ($\approx 2\ \mu$m in diameter) generated by an air nebulizer [34]. Simple calculations based on the Stokes drag formula for spherical oil droplets show little phase and amplitude distortions between flow and particle velocities for frequencies lower than a few hundred hertz [35]. Typically, the phase lag is lower than 5 deg for frequencies lower than 400 Hz. It can thus be assumed that particles follow the flow in the present experiments. Tomographic images of the droplet spray are also obtained by means of a solid-state continuous-wave YAG laser (300 mW, 532 nm) and a side-looking charge-coupled device (CCD) camera.

The geometry investigated corresponds to a scaled-up version of the small injection channels used in the DPC application [12,36]. Geometrical parameters and operating conditions defining this passive control system are gathered in the last column of Table 1. The channel diameter of 2 mm used in practice is too small to allow detailed measurements of the flow. It is, however, possible to define a larger-scale setup with operating conditions yielding Reynolds $Re = \bar{u}_0 D/\nu$ and Strouhal $St = fD/\bar{u}_0$ numbers similar to those of the

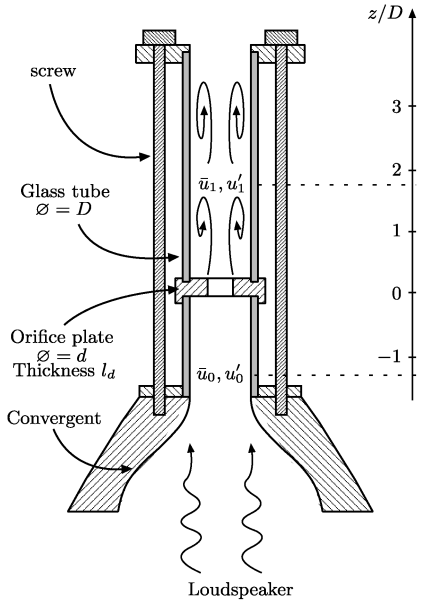

Fig. 2 Experimental setup used to study flow dynamics of an in-duct orifice plate configuration under acoustic excitation (not to scale). The gaseous stream is modulated by a driver unit (loudspeaker) placed at the bottom of the upstream manifold. The axial velocity $u = \bar{u} + u'$ is measured by LDV. Tomographic images are acquired by a side-looking CCD camera.

phase-converter device. Values corresponding to the present numerical simulations and experiments are, respectively, gathered in the first and second columns of Table 1. These parameters also conserve the dimensionless groups controlling the experimental configuration, thus fulfilling the Reynolds and Strouhal number similarity criteria.

III. Experimental Results

It is first interesting to examine visualizations of the mode conversion process using the tomographic views of the flow in Fig. 3. The five snapshots correspond to regularly spaced instants in a modulation cycle at a frequency of $f = 50$ Hz. The corresponding flow velocity is $\bar{u}_0 = 0.32\ \mathrm{m \cdot s^{-1}}$, yielding Reynolds and Strouhal numbers of $Re = 213$ and $St = 1.56$. This Strouhal number is higher than the values selected in the experiments described herein, which do not exceed 0.65. This high value is used to reveal the vortex train generated in the duct. In the tomographic images displayed in Fig. 3, the particle diameters are larger than the laser wavelength, giving rise to Mie scattering. Light scattering reaches its maximum in the forward direction, whereas radiation in the lateral direction is not uniform and the scattered light intensity is low in the perpendicular direction. To maximize light intensity, the CCD camera is placed at an angle with respect to the laser sheet and records images distorted by the perspective effect. Light rays are also deflected through the cylindrical-shaped glass tube. It is then necessary to process the raw data to eliminate these distortions. This operation is not fully accurate and the transformed images given in Fig. 3 are not precisely displayed to scale, but nevertheless the general features of the acoustically excited confined jet are provided. Vortical structures, which develop in the shear layer downstream of the orifice, are convected away by the flow at a quasi-constant velocity.

This can be confirmed by examining velocity measurements performed by means of the LDV system. The axial velocity component u is only measured with this system. Because the glass tube diameter is small and gives rise to important beam deflections, measurements are restricted to a diametral plane on which laser beams can be correctly focused. In all experiments, the analog signal delivered by the frequency counter is sampled at 16384 Hz using a 12-bit anolog–digital converter board on a PC.

A reference velocity signal $u_0(t)$ is measured at a location of $z = -1.5$ cm upstream of the orifice constriction. The response to imposed harmonic oscillations is then investigated by recording velocity signals at several streamwise locations on the duct centerline. The phase shift φ_0 is first evaluated between the reference velocity signal $u_0(t)$ and the loudspeaker signal $s(t)$: $\varphi_0 = \arg(\mathrm{S}_{u_0 s}/\mathrm{S}_{ss})$, where $\mathrm{S}_{u_0 s}$ is the cross power spectral density and S_{ss} is the power spectral density of the excitation signal. The phase shift φ_1 is then evaluated between the velocity signal $u(z, t)$ at the current location z and the loudspeaker signal $s(t)$: $\varphi_1 = \arg(\mathrm{S}_{us}/\mathrm{S}_{ss})$. The phase angle $\varphi(z)$ between the reference velocity $u_0(t)$ and the current location velocity $u(z, t)$ is finally deduced from these data:

$$\varphi(z) = \arg\left(\frac{\mathrm{S}_{us}}{\mathrm{S}_{ss}}\frac{\mathrm{S}_{ss}}{\mathrm{S}_{u_0 s}}\right) = \varphi_1 - \varphi_0 \tag{2}$$

The modulation amplitude u'_0 of the reference velocity imposed by the driver unit is fixed to $0.1\bar{u}_0$. Evolution of the phase shift $\varphi(z)$ along the setup centerline is then used to extract an axial wave number and a phase velocity using

$$c_\varphi = \frac{\omega}{k} = 2\pi f\left(\frac{\mathrm{d}\varphi}{\mathrm{d}z}\right)^{-1} \tag{3}$$

This expression provides the phase velocity of travelling perturbations on both sides of the orifice plate and can be used to define the nature of dominant perturbations. Because the flow is modulated with a loudspeaker, one expects to find acoustic and convective waves. Changes in the phase curves will reflect modifications in propagation regimes. If the propagation is of an acoustic nature, the phase velocity c_φ will be equal to the speed of sound c. If the propagation is dominated by convective perturbations, corresponding to a hydrodynamic mode, the phase velocity c_φ will be equal to the vortex convection velocity $\mathcal{U}_{\mathrm{cv}}$. In both situations, the phase will evolve linearly with the axial distance $\varphi = 2\pi f z/c_\varphi$. It is convenient to introduce the mean discharge velocity at the orifice $\bar{u}_d = \bar{u}_0/\sigma^2$,

Table 1 Geometrical parameters and flow conditions used to investigate the acoustic-hydrodynamic conversion mechanism at the duct constriction. Dimensions are expressed in meters, velocities in meters per second, and frequencies in hertz. The last column indicates the parameters defining the DPC system used to passively control combustion instabilities [11,12]

	Simulations		Experiments	DPC
Diaphragm thickness, l_d	0.5×10^{-3}		2.5×10^{-3}	0.5×10^{-3}
Channel diameter, D	2×10^{-3}		1×10^{-2}	2×10^{-3}
Orifice diameter, d	1.2×10^{-3}		6×10^{-3}	1.2×10^{-3}
Diameter ratio, $\sigma = d/D$	0.6		0.6	0.6
Inlet velocity, $\bar{u}_0$	1.94	0.32	0.5	3.5
Orifice velocity, $\bar{u}_d = \bar{u}_0/\sigma^2$	5.4	0.9	1.3	9.7
Mach, $M_d = \bar{u}_d/c$	0.016	2.7×10^{-3}	3.8×10^{-3}	0.028
Reynolds, $Re = \bar{u}_0 D/\nu$	258	213	333	466
Frequency, f	400, 600, 1000	21	16, 20, 24, 28, 32	$\simeq [400 \quad 1000]$
Strouhal, $St = fD/\bar{u}_0$	0.41, 0.62, 1.03	0.65	0.32, 0.40, 0.48, 0.56, 0.64	$\simeq [0.22 \quad 0.57]$
Strouhal, $St_d = fd/\bar{u}_d$	0.09, 0.13, 0.22	0.15	0.07, 0.09, 0.11, 0.13, 0.15	$\simeq [0.05 \quad 0.13]$

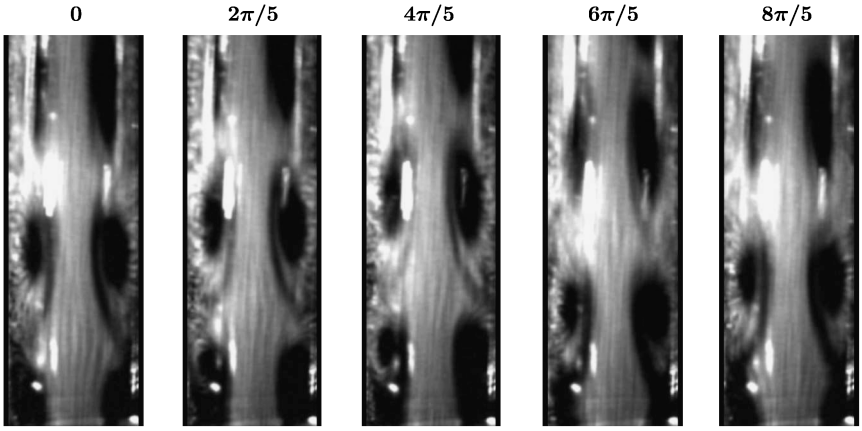

Fig. 3 Tomographic images of the unsteady flow on the downstream side of the orifice plate. Images correspond to regularly spaced phases in an oscillation cycle at $f = 50$ Hz, corresponding to a Strouhal number of $St = fD/\bar{u}_0 = 1.56$, where $\bar{u}_0 = 0.32$ m s^{-1} and $D = 1$ cm.

where $\sigma = d/D$ designates the orifice-to-duct-diameter ratio. One can then write $c_\varphi = \beta \bar{u}_d = \beta \bar{u}_0/\sigma^2$, where β is a coefficient that depends on the propagation mode. It follows that

$$\varphi = 2\pi \frac{fD}{c_\varphi}\frac{z}{D} = 2\pi \frac{1}{\beta}\frac{fD}{\bar{u}_0}\sigma^2\frac{z}{D} \tag{4}$$

or, equivalently,

$$\frac{\varphi}{2\pi St\sigma^2} = \frac{1}{\beta}\frac{z}{D} \tag{5}$$

Results are plotted in Fig. 4 using this dimensionless formulation in which the phase is divided by the product $2\pi St\sigma^2$ and represented as a function of the reduced spatial coordinate z/D (see Fig. 2). The data points nearly collapse on a single curve in the range of distances examined, confirming that the flow can be characterized with the two numbers St and σ. Some scatter is apparent for large distances from the constriction ($z/D > 1$), the slope of the curve being larger for higher values of the Strouhal number. Upstream of the orifice ($z/D < 0$), nearly vanishing phase values are obtained, which correspond to $1/\beta \ll 1$ and thus to a large phase velocity $c_\varphi \gg \bar{u}_d$. This is typical of acoustic propagation and by closely examining data in this region, it is found that the phase velocity is approximately equal to the speed of sound: $c_\varphi = c$. In the downstream region, for $z/D > 0$, the slope of the nondimensional phase $1/\beta$ is approximately equal to unity, indicating that the phase velocity c_φ is nearly equal to the mean discharge velocity $\bar{u}_d$ at the orifice. This is typical of perturbations travelling at a convection velocity ($c_\varphi = \mathcal{U}_{\rm cv} \approx \bar{u}_d$). This velocity is imposed by the vortex train shed from the orifice's sharp edges.

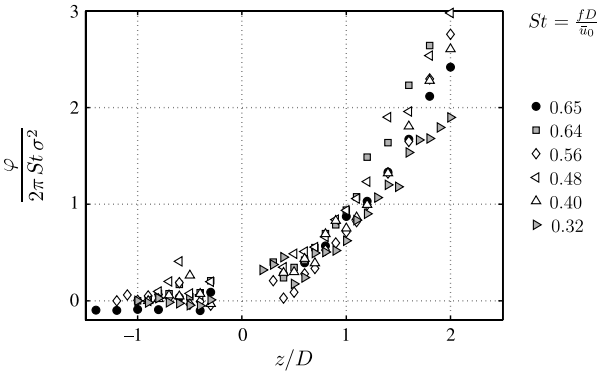

Fig. 4 Reduced phase variations as a function of the reduced axial distance z/D from the constriction orifice. The phase is obtained by comparing the velocity signal $u(z,t)$ measured on the duct centerline and a reference velocity $u_0(t)$ detected at $z/D = -1.5$. Data points correspond to Strouhal numbers $St = fD/\bar{u}_0$ comprised between 0.3 and 0.65.

IV. Numerical Simulations

It is now interesting to examine this problem with numerical simulations. The motivation is first to check that numerical flow solvers can retrieve convective modes observed experimentally. The second objective is to get the velocity field in the entire domain, which cannot be obtained experimentally and then extract the acoustic and convective components from the velocity signal. Calculations are carried out with the AVBP code developed at the European Center for Research and Advanced Training in Scientific Computation and Institut Français de Pétrole [37]. This is a Navier–Stokes flow solver operating on structured and unstructured meshes. It can be used to calculate turbulent compressible flows using large eddy simulations but also to calculate simple laminar flows, like those considered in the present paper. The flow solver precision is lower than that of direct numerical solver codes, but is sufficient for a suitable representation of the unsteady mechanisms of the modulated flow. A Lax–Wendroff second-order scheme in space and time is first used to establish the oscillating flow, and calculations are then pursued with a numerical scheme designated as TTGC, which provides third-order spatial accuracy [38].

The three-dimensional computational flow configuration is illustrated in Figs. 5 and 6. The domain geometry corresponds to one channel of the DPC system [11,12]. Dimensions are given in Fig. 6. The mesh comprises 1.66×10^6 cells and is highly refined at the duct and orifice plate walls to obtain well-resolved viscous layers. In the present configuration, the flow is laminar and one expects an axisymmetric response. This symmetry could be used to reduce the computational load, but the choice was made to allow for possible asymmetric flow dynamics and provide the groundwork for future studies at higher Reynolds numbers.

The boundary conditions used in the calculations are as follows:

1) *Inlet section*: A velocity profile fitted on the experimental data (see Fig. 7) is imposed at this boundary. The corresponding mean velocity $\bar{u}_0$ is 1.94 m $\cdot$ s^{-1}. A harmonic modulation of 10% of the amplitude of the mean flow profile is added. Three calculations are carried out for different driving frequencies (see Table 1). The injected gas is air at ambient temperature (300 K).

2) *Duct and orifice plate walls*: A no-slip adiabatic wall condition is applied on this boundary.

3) *Outlet volume coflow*: It is useful to generate a coflow around the duct to allow air entrainment and hinder the development of recirculation in the downstream volume. A steady velocity profile is imposed on this annular section with a mean velocity of 2 m $\cdot$ s^{-1} to guide the jet flowing out of the duct toward the outlet section. The velocity profile is flat from the external boundary to the duct region. It vanishes at the duct to obtain matching conditions with the no-slip duct wall boundary.

4) *Outlet volume wall*: A no-slip wall condition is imposed.

5) *Outlet section*: The domain is designed to allow the outward radiation of acoustic waves. A nonreflecting treatment applied at the

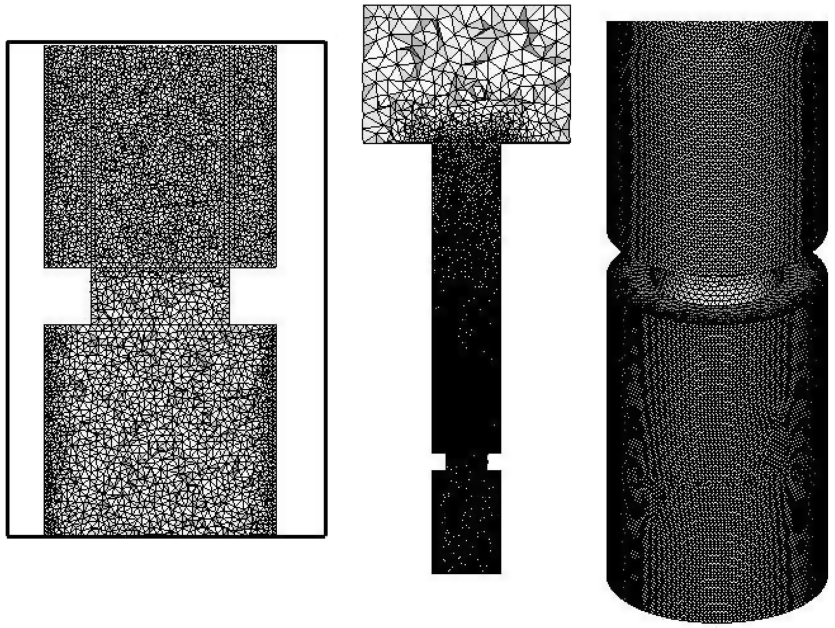

Fig. 5 System geometry and unstructured mesh used in the 3-D calculations reported in this paper: a) close-up view in the channel constricted region, b) axial slice of the entire computational domain, and c) mesh footprint on the system surface in the orifice vicinity.

outlet includes a relaxation factor that keeps the mean pressure around a predetermined ambient value [39].

After stabilization of the steady flow, the inlet velocity is modulated over at least four cycles to reach a periodic regime. Fluctuating velocity vector fields $\boldsymbol{u}'$ calculated for three different modulation frequencies (see Table 1) are displayed in Fig. 8. For each frequency, three instantaneous vector fields are shown at successive phase angles. The velocity vectors are colored by the azimuthal component of the fluctuating vorticity ς defined by

$$\varsigma = \frac{\partial u'_r}{\partial z} - \frac{\partial u'_z}{\partial r} \tag{6}$$

This quantity is deduced from the three-dimensional Cartesian velocity field issued from the calculations after transformation in cylindrical coordinates. The modulated flows corresponding to the three Strouhal numbers (0.4, 0.6, and 1) exhibit vortex shedding at the orifice lip and the subsequent convection of vortex rings. As expected, these annular structures feature different longitudinal dimensions depending on the driving frequency, and their wavelength decreases as the Strouhal number St is augmented. Confinement yields elliptical flow patterns, especially in the low-frequency cases ($f = 400$ and 600 Hz). The fluctuating vorticity takes values between -2×10^3 and 2×10^3 s^{-1}, corresponding to maximum azimuthal velocities around the vortex cores of about 1 m $\cdot$ s^{-1}. The maximum level is of the same order for the three modulation frequencies investigated. Vortex ring generation is illustrated for the highest modulation frequency $f = 1000$ Hz in Fig. 9 by plotting nine phases during a cycle of oscillation. Vorticity is identified with a Q-criterion isosurface plotted in the three dimensions, which provides a good estimation of the vortex locations [40]. The plots feature some small-scale fluctuations induced by the discrete differentiation required to estimate the Q criterion. The constant displacement of successive vortex rings between the different phases indicates that the convection velocity is constant and, in this case, approximately equal to the orifice plate discharge velocity $\mathcal{U}_{\text{cv}} \simeq \bar{u}_d = \bar{u}_0/\sigma^2$.

In the problem considered in this paper, the acoustic wavelength is large compared with the typical dimensions of the domain of interest.

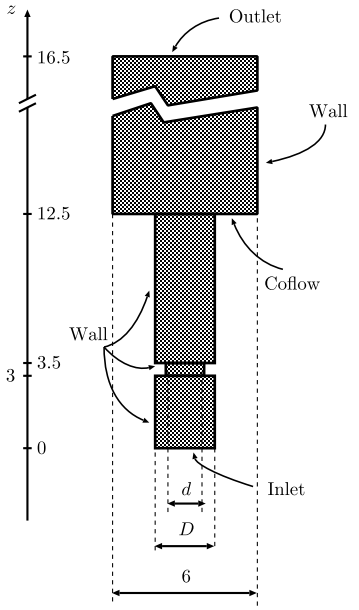

Fig. 6 Boundary conditions used in the present calculations. The figure is not drawn to scale; the dimensions are in millimeters. Inlet section: modulated velocity profile. Duct and orifice plate boundaries: No-slip conditions. Annular coflow: Constant velocity profile. Outflow volume: Slip wall condition and acoustic nonreflecting boundary for the outlet section (a coarse mesh is used in this volume).

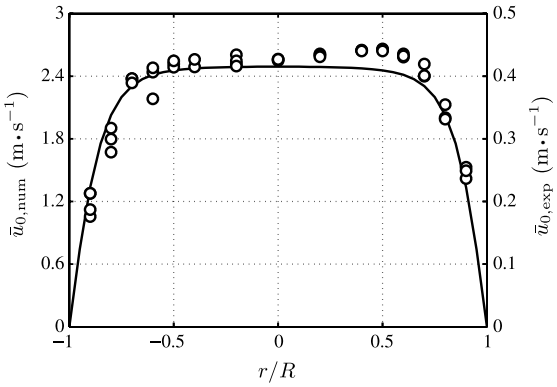

Fig. 7 Velocity profile imposed at the duct inlet. Symbols: measurements in the upstream channel of the setup described in Fig. 2. Solid line: profile used in the numerical simulations. Flow velocity: $\bar{u}_0 = 1.94$ m $\cdot$ s^{-1}.

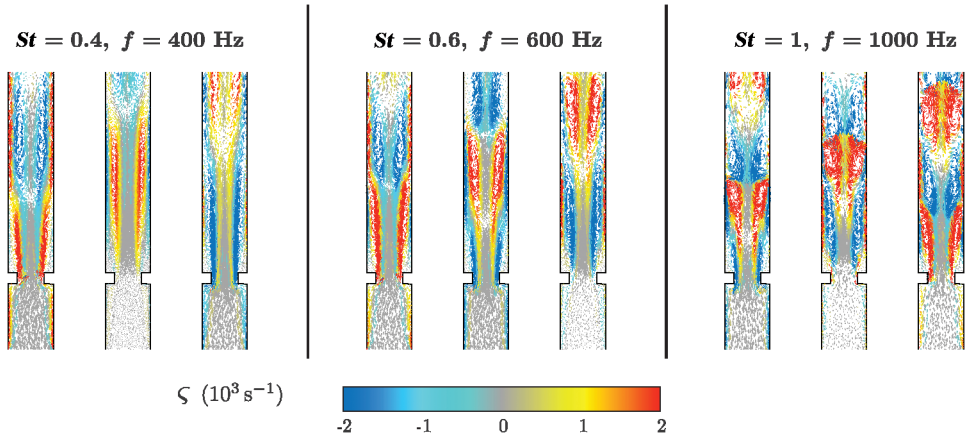

Fig. 8 Modulated flow at different forcing frequencies. Fluctuating velocity vectors are colored by the azimuthal component of the fluctuating vorticity $\varsigma = \frac{\partial u'_r}{\partial z} - \frac{\partial u'_z}{\partial r}$. Flow velocity: $\bar{u} = 1.94$ m · s^{-1}. Channel diameter: $D = 2$ mm.

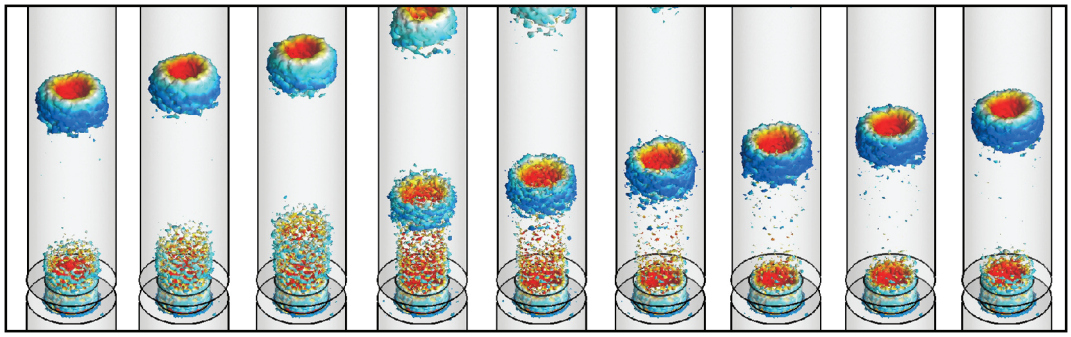

Fig. 9 Q-criterion isosurface colored by the axial velocity. The nine phases correspond to regularly spaced instants in an oscillation cycle. Modulation frequency: $f = 1000$ Hz. Flow velocity: $\bar{u}_0 = 1.94$ m · s^{-1}. Modulation amplitude: $u'_0/\bar{u}_0 = 0.1$. Channel diameter: $D = 2$ mm. Strouhal number: $St = fD/\bar{u}_0 = 1$.

The domain is acoustically compact and, there is strictly speaking no acoustical part in the problem. In this situation, the motion in the near field of the orifice can be considered to be essentially incompressible. One could then argue that there is no acoustics if the definition of acoustics is linked to compressibility (if, for instance, the sound velocity is implied in the definition). It is, however, possible to distinguish two types of motions: the first is a bulk modulation synchronized with the applied acoustic field and the second corresponds to a hydrodynamic mode generated at the orifice. Whereas the bulk mode features a nearly constant phase and propagates at a nearly infinite phase speed, the hydrodynamic mode travels at a finite phase speed corresponding to the convection velocity in the jet flow formed at the orifice. One expects that, in this case, the volume flow will be conserved over the domain of interest and the mode conversion taking place at the orifice will only modify the flow profile. Accordingly, there will be no delay in volume flow. These features are, in fact, retrieved from the simulations.

V. Acoustic-Hydrodynamic Conversion

To analyze the unsteady velocity field, it is interesting to distinguish the different types of perturbations and separate acoustic and convective components. This is done here by considering the axial fluctuating velocity component u'_z on the centerline designated as u' in the following development. On the upstream side of the orifice plate, the unsteady components of the flow are of acoustic type only. In the downstream region, the propagation mode is of mixed type with an acoustic field superimposed to the hydrodynamic fluctuations. A part of the incident acoustic energy serves to generate the train of vortices, but the energy conversion is incomplete and an unknown amount of acoustic energy remains in the downstream flow. It is then logical to try to extract the convective and acoustic components that form the velocity perturbation. Considering the velocity on the centerline, the convective fluctuating component u'_{cv} induced by vortex rings (Biot–Savart integral) can be characterized by an axial wave number k_{cv}. In the present situation, the geometrical dimensions are so small compared with the acoustic wavelengths envisaged that the acoustic velocity component can be considered to be a bulk oscillation in the vicinity of the duct constriction. For acoustic waves, propagation might take place in the two axial directions and it would be difficult to define a constant phase speed. This, however, raises no difficulty as long as the Helmholtz number $He = k_{ac}z \ll 1$ remains small and the bulk oscillation approximation is valid. For harmonic perturbations, the total centerline velocity fluctuation is then given by

$$u' = u'_{ac} + u'_{cv} = \mathcal{R}[\tilde{u}_{ac}e^{-j\omega t}] + \mathcal{R}[\tilde{u}_{cv}e^{jk_{cv}z-j\omega t}] \tag{7}$$

where $k_{cv} = \omega/\mathcal{U}_{cv}$ designates the convective wave number, $\tilde{u}_{ac}$ and $\tilde{u}_{cv}$ represent the velocity fluctuation amplitudes, and $\mathcal{R}[\ldots]$ is the real part of the complex signals. With this approximation, one may write the complex velocity signal in the following form:

$$\tilde{u}(z)e^{-j\omega t} = \tilde{u}_{ac}e^{-j\omega t} + \tilde{u}_{cv}e^{jk_{cv}z-j\omega t} \tag{8}$$

where $\tilde{u}(z)$ is the complex amplitude of the harmonic velocity fluctuation $u'(z,t) = \mathcal{R}[\tilde{u}(z)e^{-j\omega t}]$. The discrimination between the bulk oscillation due to acoustic propagation and the convective mode induced by downstream vortices is based on the very different phase velocities associated with these modes.

It is now possible to extract the bulk and convective components $\tilde{u}_{ac}$ and $\tilde{u}_{cv}$ and the convective wave number k_{cv} from the simulation as follows. The procedure uses the velocity data at a set of discrete points on the z axis in combination with an analytic signal representation of these velocity fluctuations. In what follows, $u'_i(t) =$

$u'(z_i, t)$ corresponds to the fluctuating velocity signal at the centerline location z_i, $i = 1, \ldots, N$.

1) For the set of streamwise locations z_i on the central axis, an analytic representation of the velocity fluctuation $\hat{u}_i$ is constructed by taking the Hilbert transform of the real velocity signal $u'_i(t)$ provided by the simulations:

$$\hat{u}_i = u'_i + j\mathcal{H}(u'_i) \tag{9}$$

where $\mathcal{H}$ denotes the Hilbert transform. This representation is often used in signal processing to demodulate narrow band signals including a carrier and a message. One thus obtains a complex representation $\hat{u}_i(t)$ of the real fluctuating signal $u'_i(t)$.

2) Because bulk and convective components are harmonic functions, the analytical representation $\hat{u}_i(t)$ is also a time harmonic function: $\hat{u}_i = \tilde{u}_i e^{-j\omega t}$. Now, the complex amplitude $\tilde{u}_i$ of this signal is identified with the components appearing in Eq. (8):

$$\tilde{u}_i = \tilde{u}_{i,\mathrm{ac}} + \tilde{u}_{i,\mathrm{cv}} e^{jk_{i,\mathrm{cv}} z_i} \tag{10}$$

where $\tilde{u}_{i,\mathrm{ac}}$, $\tilde{u}_{i,\mathrm{cv}}$, and $k_{i,\mathrm{cv}}$ denote local values for the bulk and convective fluctuations and the convective wave number, respectively.

3) Assuming that preceding quantities remain constant over the spatial range $[z_{i-1},\ z_{i+1}]$, it is possible to derive expressions for $\tilde{u}_{i,\mathrm{ac}}$ and $\tilde{u}_{i,\mathrm{cv}}$ as functions of the three complex values $\tilde{u}_{i-1}$, $\tilde{u}_i$, and $\tilde{u}_{i+1}$. This can be done by noting that these values belong to a common circle in the complex plane. The center is at $\tilde{u}_{i,\mathrm{ac}}$ and the radius equals $|\tilde{u}_{i,\mathrm{cv}}|$.

4) The last unknown $k_{i,\mathrm{cv}}$ is easily retrieved by substituting the values obtained for $\tilde{u}_{i,\mathrm{ac}}$ and $|\tilde{u}_{i,\mathrm{cv}}|$ in the previous step in Eq. (10) written for $i-1$, i, or $i+1$. This can also be used to crosscheck the results.

This process provides the bulk and convective fluctuating velocities and the wave number as a function of the axial coordinate z. It is important to note that the choice of the spatial step discretization Δz results from a tradeoff. If the spatial sampling z_i is too coarse, assumptions made on the unknowns' uniformity over the span $[z_{i-1},\ z_{i+1}]$ are invalid. If the spatial sampling is too refined, the three complex values $\tilde{u}_{i-1}$, $\tilde{u}_i$, and $\tilde{u}_{i+1}$ are too close on the common circle, leading to large uncertainties in the determination of $\tilde{u}_{i,\mathrm{ac}}$ and $\tilde{u}_{i,\mathrm{cv}}$.

It is not too difficult to deal with this tradeoff and adjust the parameters to obtain reliable estimates. The followings results were obtained for a sampling $\Delta z/D = 0.25$ from $z/D = -1$ to $z/D = 2.5$ by postprocessing the different cases presented in Fig. 8. It is worth examining first the evolution of the mean centerline velocity $\bar{u}(z)$ plotted in Fig. 10. This quantity is extracted from time evolution signals over four periods of oscillation. For axial locations $z/D \leq -1$, the mean velocity $\bar{u}(z)$ takes a constant value equal to that imposed at the duct inlet $\bar{u}(z/D = -1) \simeq 2.5\ \mathrm{m \cdot s^{-1}}$ (see Fig. 7). It then rapidly increases within 1 diameter to reach its maximum value at the constriction location $\bar{u}(z/D = 0) \simeq 9\ \mathrm{m \cdot s^{-1}}$. The orifice plate is located at $z/D = 0$. The centerline velocity then slowly decreases away from the constriction in the downstream direction. It would eventually reduce to the bulk flow velocity $\bar{u}_0$ once the vortices are dissipated further downstream, but this was not checked due to the limited size of the computational domain.

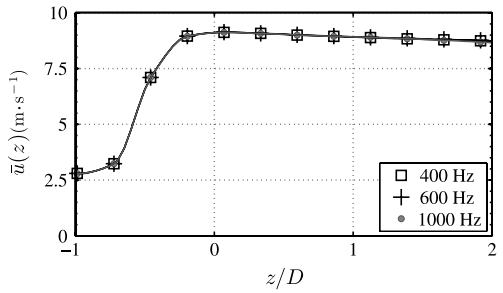

Fig. 10 Mean centerline velocity profile $\bar{u}(z)$ in the vicinity of the constriction located at $z/D = 0$. The bulk flow velocity in the duct is $\bar{u}_0 = 1.94\ \mathrm{m \cdot s^{-1}}$.

Time traces of the axial velocity fluctuation component u' on the centerline axis are examined in Fig. 11 for a modulation at $f = 600$ Hz. The set of plots in these figures corresponds to different axial locations z/D. Brighter plots indicate increasing axial locations. The set of raw fluctuating velocity signals in Fig. 11a features different time lags within an envelope for the amplitude. Convective modes are responsible for these times lags whereas the envelope is due to the bulk oscillation associated with the acoustic component of the fluctuating velocity, as will be shown next. The extracted acoustic components of the raw signals are displayed in Fig. 11b. Dark lines corresponding to time traces in the region upstream of the constriction ($z/D < 0$) are all superimposed, indicating that the acoustic component impinging on the constriction is barely affected by its presence on the upstream side. Bright lines correspond to time traces in the downstream region of the constriction $z/D > 0$. They also barely collapse into a single curve, but with a reduced amplitude of oscillation. This indicates that the bulk oscillation associated with the acoustic velocity fluctuation is suddenly diminished at the constriction location. Extracted convective components are displayed in Fig. 11c. This component is absent upstream of the constriction (dark lines) and becomes dominant in the downstream region (bright lines). It is found that a rapid conversion of acoustic to hydrodynamic perturbations takes place at the constriction and that the amplitude of the convective component is progressively amplified.

Using the same processing method, results are now presented in Fig. 12 as a function of the reduced spatial coordinates z/D. The relative fluctuation velocity signals are plotted in Fig. 12a at eight instants in an oscillation cycle indicated by different gray levels. Amplitudes of extracted acoustic and convective velocity compo-

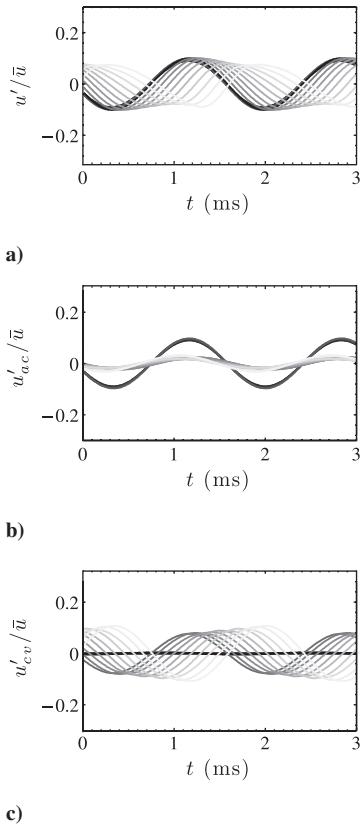

Fig. 11 Time traces of normalized velocity fluctuations $u'(z_i, t)/\bar{u}(z_i)$ at different axial locations z_i: a) raw fluctuating velocity signals u', b) extracted acoustic component u'_{ac}, and c) extracted convective component u'_{cv}. Simulation: $f = 600$ Hz, $\bar{u}_0 = 1.94\ \mathrm{m \cdot s^{-1}}$, and $D = 2$ mm. The darkness of the plots indicates increasing axial locations from $z/D = -1$ (dark line) to $z/D = 2.5$ (white line).

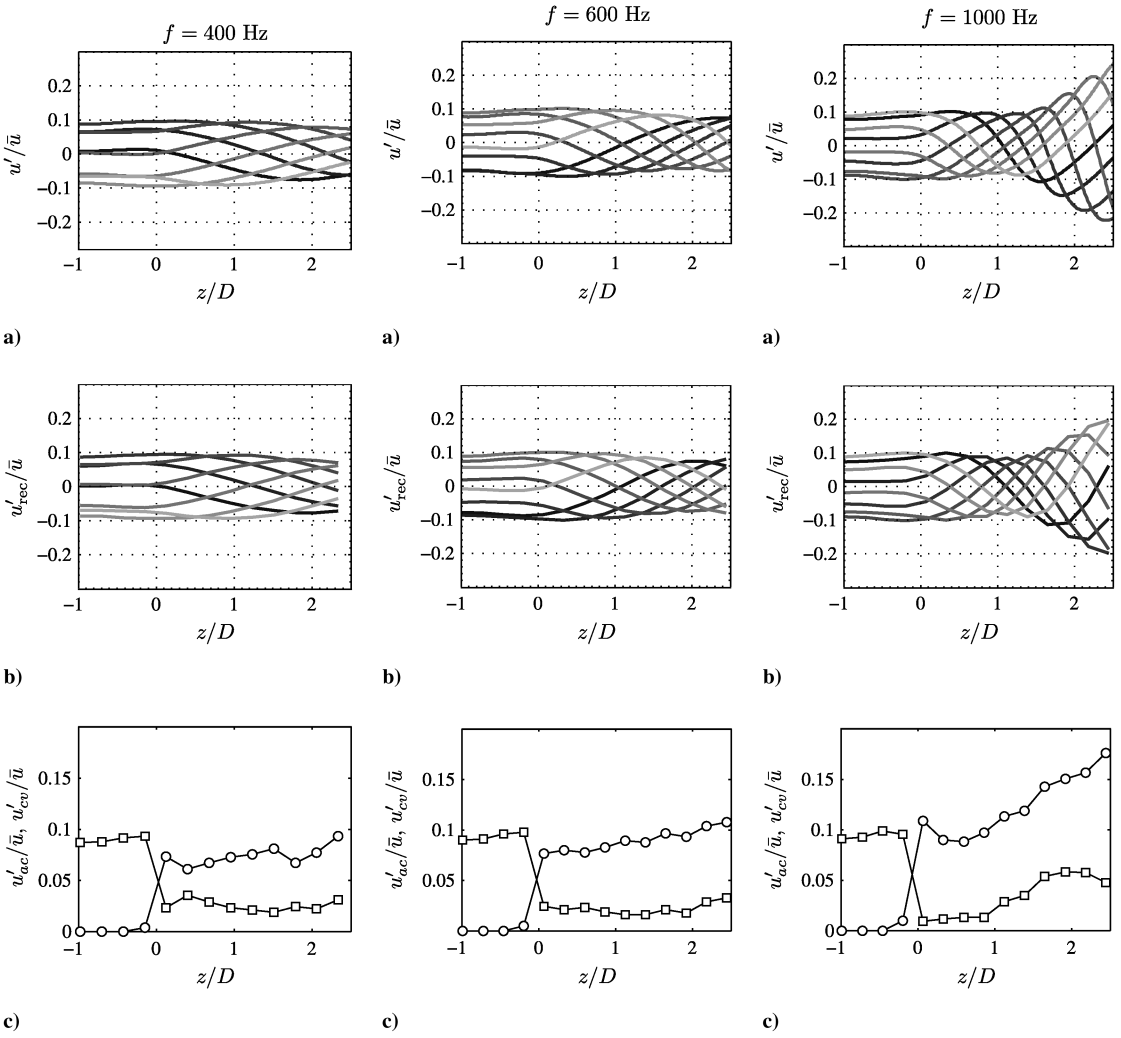

Fig. 12 Spatial representation of centerline velocity fluctuations: a) raw signals; and b) signals reconstructed from the extracted acoustic velocities $\tilde{u}_{ac}$, convective velocities $\tilde{u}_{cv}$, and convective wave number k_{cv} (the darkness indicates different instants in the oscillation cycle); and c) extracted amplitudes of acoustic □ and convective ○ components. Results are normalized by the local value of the mean centerline velocity $\bar{u} = \bar{u}(z_i)$ given in Fig. 10.

nents are given in Fig. 12c. These components are then used together with the phase velocity to reconstruct the velocity time traces shown in Fig. 12b. These reconstructed signals closely reproduce the raw data indicating that the wave extraction method described previously effectively decomposes the perturbation in its components. For the three cases explored, one notices that the velocity fluctuation amplitude remains constant in the upstream region ($z/D < 0$) and is of bulk oscillation type. A wavelike pattern is observed in the downstream region of the orifice, which is dominated by convective perturbations. The mode conversion process taking place at the orifice is well highlighted in Fig. 12c. It is interesting to note that this process yields a relative convective velocity perturbation that is about equal to the relative acoustic perturbation $u'_{ac}/\bar{u}(z) = \eta u'_{cv}/\bar{u}(z)$, where η is a conversion efficiency that is, in the present case, of the order of unity and $\bar{u}(z)$ designates the mean centerline velocity in the local section. It is probable that η depends on the geometry of the orifice plate and also, to some extent, on the Strouhal number $\eta = \eta(\sigma; St)$, but this has not been investigated. Now, because the mean flow is incompressible, the mean centerline velocity $\bar{u}(z)$ remains constant in the upstream region and increases sharply at the diaphragm by a factor of $1/\sigma^2$ (see Fig. 10). This yields a simple relation between the velocity fluctuations on the two sides of the constriction: $u'_{cv} \simeq u'_{ac}/\sigma^2$. Another interesting feature is that the amplitude of the convective component increases in the downstream direction, and this is particularly visible at the highest modulation frequency of $f = 1000$ Hz. This can be interpreted in terms of a hydrodynamic stability analysis, which indicates that perturbations are amplified and that this process is most effective for jet Strouhal numbers of the order of 0.3. It turns out that the Strouhal number based on the orifice diameter and the discharge velocity, $St_d = fd/\bar{u}_d$, is, in this case, 0.216, which is not far from the preferred value for freejets. The growth of the convective component on the jet axis is also well observed in similar experiments carried out on freejets [13].

It is next interesting to examine the convective wave number k_{cv} and deduce from this quantity the evolution of the convective velocity of vortices $\mathcal{U}_{cv}$ along the centerline axis using Eq. (3):

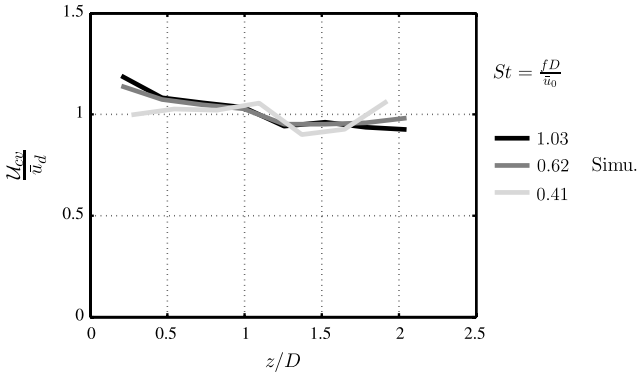

Fig. 13 Evolution of the vortex convection velocity $\mathcal{U}_{cv}$ normalized by the discharge velocity $\bar{u}_d = \bar{u}_0/\sigma^2$ as a function of the normalized distance to the constriction z/D. $\bar{u}_0 = 1.94$ m · s^{-1}, $D = 2$ mm, and $\sigma = d/D = 0.6$.

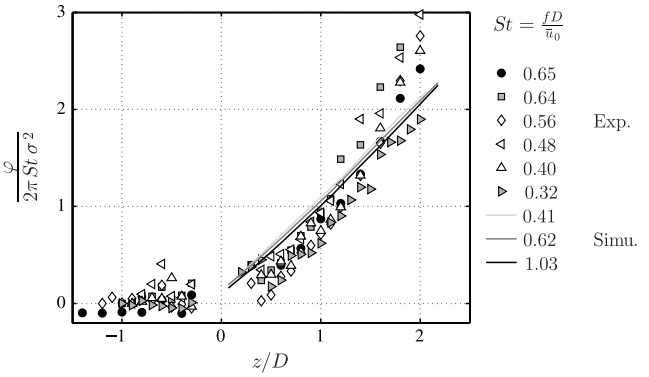

Fig. 14 Reduced phase variations as a function of reduced distances to the constriction. Symbols: experiments. Solid lines: results of numerical simulations.

$\mathcal{U}_{cv} = 2\pi f/k_{cv}(z) = 2\pi f(\mathrm{d}\varphi/\mathrm{d}z)^{-1}$. This is done in Fig. 13, which shows that the ratio $\mathcal{U}_{cv}/\bar{u}_d$ remains close to 1 for the range of Strouhal numbers explored (0.4–1.0). The convection velocity does not depend on the forcing frequency and is nearly equal to the orifice mean discharge velocity $\bar{u}_d = \bar{u}_0/\sigma^2$. The corresponding phase shift may then be deduced from the values of $\mathcal{U}_{cv}$ ($\varphi = \omega z/\mathcal{U}_{cv}$) and plotted in Fig. 14 using the reduced coordinates employed in the experimental data reduction [Eq. (5)]. Phase shifts obtained numerically follow the experimental data points, confirming the validity of the correlation established earlier.

Finally, it is worth examining if the mode conversion process gives rise to nonuniform modulations of the volume flow rate. It is clear that the mean flow is incompressible because the flow Mach number is low $M = \bar{u}/c \ll 1$. But the constriction induces the shedding of coherent vortex rings when the flow is acoustically modulated, and these convective structures generate large flow perturbations downstream of the constriction. Hydrodynamic velocity perturbations induced by these structures on the centerline exhibit convective wavelike patterns as shown in Fig. 12 in the downstream region of the orifice plate whereas the bulk oscillation due to acoustics is reduced. However, it is important to remember that this only describes the fluid motion on the centerline. Whereas the acoustic flow is one dimensional, hydrodynamic perturbations in the downstream region correspond to three-dimensional ringlike vortices. In a given cross section downstream of the constriction, convective axial velocity perturbations will be positive or negative depending on the radial location in the duct, but the net volume flow rate remains essentially constant. This is demonstrated in Fig. 15, in which the evolution of the fluctuating volume flow rate $\dot{V}'$, calculated by integrating the volumetric flux over the duct cross section, is plotted as a function of the axial location z/D. It is shown that there is no delay or attenuation of the volume flow rate fluctuation on the downstream side of the constriction. This is an important aspect when considering injection systems fed with reactants. The response of such orifice plates to acoustic perturbations does not change the supply of reactants, but only modifies the velocity field distribution. Part of the energy conveyed by the bulk oscillation motion is transferred to the hydrodynamic perturbation. Although the volume flow rate oscillation remains unchanged because the flow is incompressible, mode conversion has occurred and the resulting vortices are eventually dissipated further downstream, leaving an acoustic modulation of a reduced amplitude.

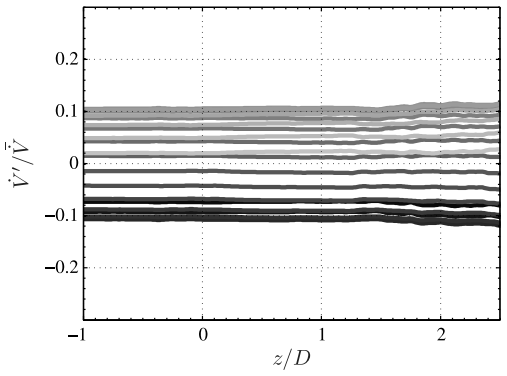

Fig. 15 Evolution of the normalized fluctuations of the volume flow rate with the reduced distance to the constriction. Simulation: $f = 600$ Hz, $\bar{u}_0 = 1.94\ \mathrm{m \cdot s^{-1}}$, $D = 2$ mm, and $St = 0.6$. The darkness indicates different instants in the oscillation cycle.

VI. Conclusions

The dynamics of confined jets established in a duct by an orifice plate is examined in this paper for low Reynolds flows. The system is submitted to large pressure oscillations that are converted by the orifice into a convective mode. Combined experiments and numerical simulations indicate the following.

1) It is possible to collapse phase data by making use of a normalized phase and a reduced axial coordinate and to extract the same scaling rules from the experimental data and from numerical simulations.

2) The convection velocity of vortices generated in the confined jet by external modulations of the flow is equal to the mean discharge velocity at the orifice plate. This result holds for a broad range of frequencies: $\mathcal{U}_{cv} \simeq \bar{u}_0/\sigma^2$, where $\bar{u}_0$ is the mean flow velocity in the duct.

3) Digital processing based on the Hilbert transform can be used to extract acoustic and convective components from the centerline velocity signals, yielding an interesting description of the mode conversion process taking place at the orifice lip.

4) The incident acoustic perturbations generate three-dimensional, nearly axisymmetric vortex rings. In the geometry investigated corresponding to an orifice-to-duct-diameter ratio of $\sigma = 0.6$, the convective component on the centerline and on the downstream side of the orifice plate is about equal to the incident acoustic velocity fluctuation divided by the orifice-to-duct-section ratio $u'_{cv} \simeq u'_{ac}/\sigma^2$. The conversion efficiency is high; it modifies the perturbed velocity distribution but does not induce volume flow rate modulations.

This type of system may be placed in reactant injection channels to control the response of flames to flow oscillations, a principle explored in multipoint burners to damp collective flame effects. This provides an effective way to produce flow perturbations of shorter wavelengths when subjected to the acoustic excitations of large wavelengths.

Acknowledgments

Experiments in this investigation were carried out in part by Julien Belliato and Adrien Nicoletis, Master's students at the Ecole Centrale Paris.

References

[1] Ho, C.-M., and Huerre, P., "Perturbed Free Shear Layer," *Annual Review of Fluid Mechanics*, Vol. 16, 1984, pp. 365–424. doi:10.1146/annurev.fl.16.010184.002053

[2] Plett, E., and Summerfield, M., "Jet Engine Exhaust Noise Due to Rough Combustion and Nonsteady Aerodynamic Sources," *Journal of the Acoustical Society of America*, Vol. 56, No. 2, 1974, pp. 516–522. doi:10.1121/1.1903285

[3] Pickett, G., *Core Engine Noise Due to Turbine Fluctuations Convecting Through Turbine Blade Rows*, Progress in Astronautics and Aeronautics, Vol. 43, AIAA, New York, 1976, pp. 589–608.

[4] Marble, F., and Candel, S., "Acoustic Disturbances from Gas Nonuniformities Convected Acoustic Disturbances from Gas Nonuniformities Convected Through a Nozzle," *Journal of Sound and Vibration*, Vol. 55, 1977, pp. 225–243. doi:10.1016/0022-460X(77)90596-X

[5] Cumpsty, N., and Marble, F., "The Interaction of Entropy Fluctuations with Turbine Blade Rows; A Mechanism of Turbojet Engine Noise," *Proceedings of the Royal Society A. Mathematical, Physical and Engineering Sciences*, Vol. 357, 1977, pp. 323–344. doi:10.1098/rspa.1977.0171

[6] Crow, S., and Champagne, F., "Orderly Structure in Jet Turbulence," *Journal of Fluid Mechanics*, Vol. 48, 1971, pp. 547–591. doi:10.1017/S0022112071001745
[7] Juvé, D., Sunyach, M., and Comte-Bellot, G., "Intermittency of Noise Emission in Subsonic Cold Jets," *Journal of Sound and Vibration*, Vol. 71, 1980, pp. 319–332. doi:10.1016/0022-460X(80)90416-2
[8] Zaman, K., "Far-Field Noise of a Subsonic Jet Under Controlled Excitation," *Journal of Fluid Mechanics*, Vol. 152, 1985, pp. 83–111. doi:10.1017/S0022112085000581
[9] Hughes, I. J., and Dowling, A. P., "The Absorption of Sound by Perforated Linings," *Journal of Fluid Mechanics*, Vol. 218, 1990, pp. 299–335. doi:10.1017/S002211209000101X
[10] Eldredge, J. D., and Dowling, A., "The Absorption of Axial Acoustic Waves by a Perforated Liner with Bias Flow," *Journal of Fluid Mechanics*, Vol. 485, 2003, pp. 307–335. doi:10.1017/S0022112003004518
[11] Noiray, N., Durox, D., Schuller, T., and Candel, S., "A Novel Strategy for Passive Control of Combustion Instabilities," American Society of Mechanical Engineers Paper GT2008-51520, 2008.
[12] Noiray, N., Durox, D., Schuller, T., and Candel, S., "Dynamic Phase Converter for Passive Control of Combustion Instabilities," *Proceedings of the Combustion Institute*, Vol. 32, 2009, pp. 3163–3170. doi:10.1016/j.proci.2008.05.051.
[13] Birbaud, A. L., Durox, D., Ducruix, S., and Candel, S., "Dynamics of Free Jets Submitted to Upstream Acoustic Modulations," *Physics of Fluids*, Vol. 19, No. 1, 2007, pp. 013602. doi:10.1063/1.2432156
[14] Hirschberg, A., *Introduction to Aero-Acoustics of Internal Flow*, Advances in Aeroacoustics, Vol. 2, von Karman Institute for Fluid Dynamics, Rhode-St-Genèse, Belgium, 2001.
[15] Zhao, W., Frankel, S. H., and Mongeau, L., "Numerical Simulations of Sound from Confined Pulsating Axisymmetric Jets," *AIAA Journal*, Vol. 39, No. 10, 2001, pp. 1868–1874. doi:10.2514/2.1201
[16] Griffith, M., Leweke, T., Thompson, M., and Hourigan, K., "Blockage Effects on Steady and Pulsatile Flows in Stenotic Geometries," *American Physical Society Meeting Abstracts*, American Physical Society, College Park, MD, Nov. 2006, pp. GA.007.
[17] Durrieu, P., Hofmans, G., Ajello, G., Boot, R., Auregan, Y., Hirschberg, A., and Peters, M. C. A. M., "Quasisteady Aero-Acoustic Response of Orifices," *Journal of the Acoustical Society of America*, Vol. 110, No. 4, 2001, pp. 1859–1872. doi:10.1121/1.1398058
[18] Hofmans, G. C. J., Ranucci, M., Ajello, G., Auregan, Y., and Hirschberg, A., "Aeroacoustic Response of a Slit-Shaped Diaphragm in a Pipe at Low Helmholtz Number, 1: Quasi-Steady Results," *Journal of Sound and Vibration*, Vol. 244, No. 1, 2001, pp. 35–56. doi:10.1006/jsvi.2000.3457
[19] Hofmans, G. C. J., Ranucci, M., Ajello, G., Auregan, Y., and Hirschberg, A., "Aeroacoustic Response of a Slit-Shaped Diaphragm in a Pipe at Low Helmholtz Number, 2: Unsteady Results," *Journal of Sound and Vibration*, Vol. 244, No. 1, 2001, pp. 57–77. doi:10.1006/jsvi.2000.3458
[20] Leung, R. C. K., So, R. M. C., Wang, M. H., and Li, X. M., "In-Duct Orifice and Its Effect on Sound Absorption," *Journal of Sound and Vibration*, Vol. 299, 2007, pp. 990–1004. doi:10.1016/j.jsv.2006.08.001
[21] Fabignon, Y., Dupays, J., Avalon, G., Vuillot, F., Lupoglazoff, N., Casalis, G., and Prévost, M., "Instabilities and Pressure Oscillations in Solid Rocket Motors," *Aerospace Science and Technology*, Vol. 7, 2003, pp. 191–200. doi:10.1016/S1270-9638(02)01194-X
[22] Culick, F. E. C., *Unsteady Motions in Combustion Chambers for Propulsion Systems*, NATO/RTO-AGAVT-039, AGARD, Neuilly-sur-Seine, France, 2006.
[23] Flandro, G. A., "Vortex Driving Mechanism in Oscillatory Rocket Flows," *Journal of Propulsion and Power*, Vol. 2, No. 3, 1986, pp. 206–214. doi:10.2514/3.22871
[24] Vuillot, F., "Vortex-Shedding Phenomena in Solid Rocket Motors," *Journal of Propulsion and Power*, Vol. 11, No. 4, 1995, pp. 626–639. doi:10.2514/3.23888
[25] Anthoine, J., Mettenleiter, M., Repellin, O., Buchlin, J.-M., and Candel, S., "Influence of Adaptative Control On Vortex-Driven Instabilities in a Scaled Model of Solid Propellent Motors," *Journal of Sound and Vibration*, Vol. 262, 2003, pp. 1009–1046. doi:10.1016/S0022-460X(02)01034-9
[26] Rossiter, J. E., "Wind Tunnel Experiments on the Flow over Rectangular Cavities at Subsonic and Transonic Speeds," Aeronautical Research Council, Ministry of Aviation, Rept. ARC/R&M-3438, London, 1964.
[27] Bechert, D., "Sound Absorption Caused by Vorticity Shedding, Demonstrated with a Jet Flow," *Journal of Sound and Vibration*, Vol. 70, 1980, pp. 389–405. doi:10.1016/0022-460X(80)90307-7
[28] Wendoloski, J. C., "Sound Absorption by an Orifice Plate in a Flow Duct," *Journal of the Acoustical Society of America*, Vol. 104, No. 1, 1998, pp. 122–132. doi:10.1121/1.423262
[29] Howe, M. S., "On the Theory of Unsteady High Reynolds Number Flow Through a Circular Aperture," *Proceedings of the Royal Society A. Mathematical, Physical and Engineering Sciences*, Vol. 366, 1979, pp. 205–223. doi:10.1098/rspa.1979.0048
[30] Cummings, A., and Eversman, W., "High Amplitude Acoustic Transmission Through Duct Terminations: Theory," *Journal of Sound and Vibration*, Vol. 91, No. 4, 1983, pp. 503–518. doi:10.1016/0022-460X(83)90829-5
[31] Dupére, I. D. J., and Dowling, A. P., "The Absorption of Sound Near Abrupt Axisymmetric Area Expansions," *Journal of Sound and Vibration*, Vol. 239, No. 4, 2001, pp. 709–730. doi:10.1006/jsvi.2000.3224
[32] Saffman, P. G., *Vortex Dynamics*, Cambridge Univ. Press, Cambridge, England, U.K., 1992.
[33] Cummings, A., "The Effects of Grazing Turbulent Pipe-Flow on the Impedance of an Orifice," *Acustica*, Vol. 61, No. 4, 1986, pp. 233–242.
[34] Durox, D., Ducruix, S., and Lacas, F., "Flow Seeding with an Air Nebulizer," *Experiments in Fluids*, Vol. 27, 1999, pp. 408–413. doi:10.1007/s003480050365
[35] Albrecht, H.-E., Damaschke, N., Borys, M., and Tropea, C., *Laser Doppler and Phase Doppler Measurement Techniques*, Springer–Verlag, Berlin, 2003.
[36] Noiray, N., Durox, D., Schuller, T., and Candel, S., "A Unified Framework for Nonlinear Combustion Instability Analysis Based on the Flame Describing Function," *Journal of Fluid Mechanics*, Vol. 615, 2008, pp. 139–167. doi:10.1017/S0022112008003613
[37] Schönfeld, T., and Rudgyard, M., "Steady and Unsteady Flow Simulations Using the Hybrid Flow Solver AVBP," *AIAA Journal*, Vol. 37, No. 11, 1999, pp. 1378–1385. doi:10.2514/2.636
[38] Colin, O., and Rudgyard, M., "Development of High-Order Taylor-Galerkin Schemes for LES," *Journal of Computational Physics*, Vol. 162, No. 2, 2000, pp. 338–371. doi:10.1006/jcph.2000.6538
[39] Poinsot, T., and Veynante, D., *Theoretical and Numerical Combustion*, Edwards, Philadelphia, 2001.
[40] Haller, G., "An Objective Definition of a Vortex," *Journal of Fluid Mechanics*, Vol. 525, 2005, pp. 1–26. doi:10.1017/S0022112004002526

J. Astley
Associate Editor